Photosensitizer effects on cancerous cells: A combined study using synchrotron infrared and fluorescence microscopies

Sirinart Chio-Srichan, Matthieu Refregiers, Frederic Jamme, Slavka Kascakova, Valérie Rouam, Paul Dumas

Photosensitizer effects on cancerous cells: A combined study using synchrotron infrared and fluorescence microscopies

Sirinart Chio-Srichan, Matthieu Refregiers, Frederic Jamme, Slavka Kascakova, Valérie Rouam, Paul Dumas

PII: S0304-4165(08)00039-1
DOI: doi: 10.1016/j.bbagen.2008.02.004
Reference: BBAGEN 26512

To appear in: *BBA - General Subjects*

Received date: 19 December 2007
Revised date: 8 February 2008
Accepted date: 11 February 2008

Please cite this article as: Sirinart Chio-Srichan, Matthieu Refregiers, Frederic Jamme, Slavka Kascakova, Valérie Rouam, Paul Dumas, Photosensitizer effects on cancerous cells: A combined study using synchrotron infrared and fluorescence microscopies, *BBA - General Subjects* (2008), doi: 10.1016/j.bbagen.2008.02.004

Photosensitizer Effects on Cancerous Cells: a combined study using synchrotron infrared and fluorescence microscopies.

Ms Sirinart Chio-Srichan[a], Dr Matthieu Refregiers[a], Dr Frederic Jamme[a,b], Dr Slavka Kascakova[c], Ms Valérie Rouam[a], Dr Paul Dumas[a]

[a]Synchrotron SOLEIL, L'Orme des Merisiers, Saint-Aubin, 91192 Gif-sur-Yvette, France

[b] CEPIA, Insitut National de la Recherche Agronomique (INRA), 44316 Nantes, France

[c] Department of Biophysics, P. J. Safarik University, Kosice, Slovakia

Corresponding author: Matthieu Refregiers, matthieu.refregiers @synchrotron-soleil.fr

DISCO, SOLEIL Synchrotron, L'orme des Merisiers, 91192 GIF SUR YVETTE cédex, FRANCE

phone : 33 1 69359655

fax : 33 1 69359456

Keywords: hypocrellin, infrared, fluorescence, microscopy, synchrotron, photodynamic therapy, cancer cells

SUMMARY

Hypocrellin A (HA), a lipid-soluble peryloquinone derivative, isolated from natural fungus sacs of *Hypocrella bambusae*, has been reported to be a highly potential photosensitizer in photodynamic therapy (PDT). It has been studied increasingly because of its anticancer activities when irradiated with light. We have studied the interaction mechanisms of HA with HeLa cells as a function of incubation time. Fluorescence microscopy confirmed that HA localization is limited in the cytoplasm before eventually concentrating in clusters around the nucleus. The IR spectra of HA treated-, PDT treated- and control- HeLa cells were recorded at the ESRF Infrared beamline (ID21). Principal component analysis has been used to assess the IR spectral changes between the various HeLa cells spectral data sets (The Unscrambler software, CAMO). PCA revealed that there is a frequency shift of protein amide I and amide II vibrational bands, indicating changes in the protein secondary structures of the HA treated- and PDT treated- cancer cells compared to the control cells. In addition, the relative DNA intensity in HA treated cells decreases gradually along the incubation time. The use of synchrotron infrared microscopy is shown to be of paramount importance for targeting specifically the biochemical modification induced in the cell nucleus.

INTRODUCTION

Photodynamic therapy (PDT) has exhibited an increasing interest as a potential cancer treatment in the recent years. The principle of this therapy is based upon the interaction of light with a photosensitizer, which, in turn, results in the production of radical species inducing the death of cancerous cells and infectious organisms [1]. Photodynamic effects inducing the death of cancer cells are suggested to proceed along two main pathways e.g. the production of active free radicals by electron proton transfer reaction with biomolecules (Type I) and/or the production of singlet oxygen when the photosensitizer transfers the energy to oxygen (Type II) [2]. Both pathways require light to excite the photosensitizer and also oxygen to generate active species via radical chain reaction [3].

Up to now, Photofrin® is the only photosensitizer approved by the European Union and the United States FDA and Asian countries [4]. Other compounds have been investigating as alternatives such as hypocrellins, hypericin, porphyrin etc. Hypocrellin A (HA) (Fig.1), a natural hydrophobic peryloquinone derivative isolated from natural fungus sacs of *Hypocrella bambusae*, has gained considerable interest since its anticancer and antiviral activities especially HIV-1 have been reported [5-7]. HA has been used in Chinese traditional medicine for several hundred years [8]. HA can cause cell damage by both photodynamic type I reaction (with the active oxygen species (O_2, $O^{\cdot-}_2$) and type II reaction (with the hypocrellin radicals such as semiquinone radical anions ($HA^{\cdot-}$, $HB^{\cdot-}$) [9]. As singlet oxygen has a very short lifetime in the nucleus, the PDT action may occur close to or in the organelles of hypocrellin localisation. Many studies have been performed by using

fluorescent properties of hypocrellin for investigating its cellular uptake and its intracellular distribution inside the cell. It has been, then shown that mitochondria, lysosome, and the Golgi apparatus are the targets of PDT [10, 11]. Fluorescence spectroscopy and microscopy are established techniques for following molecules inside cells and tissues.

Vibrational spectroscopy is able to detect specific biochemical changes within tissues [12-14]. It carries a high level of molecular information but, with a spatial resolution limited by the weakness of the laboratory source (at a scale of several tens of square microns). The addition of a microscope as an accessory to conventional Fourier Transform InfraRed (FTIR) spectrometers has brought the potential to examine tissues at cellular resolution. It has led to infrared imaging, where biochemical and spatial information are combined [15]. Since the vibrational fingerprints of many common biological molecules such as lipids, proteins, carbohydrates and nucleic acids, are available and can be accessed to investigate the biological samples, this technique becomes more and more used by biological and biomedicine researchers [12, 16].

It appears quite clear, nowadays, that both infrared spectroscopy and microscopy are markedly contributing to our understanding of cancer based on chemical changes detected by infrared spectroscopy rather than based on morphological features of a cell. One important challenge is to use this approach to reveal earlier forms of cancer, which could direct the study of cancer to as of yet unrecognized premalignant forms that could allow a more radical treatment once they are diagnosed.

There is, nowadays, a tremendous interest on infrared microscopy, not with a conventional blackbody (thermal) source, but with a synchrotron radiation source.

The advantage of the synchrotron has provided a tremendous step forward in the analysis of biological components in the cell at sub-cellular resolution [17, 18]. The spatial resolution, thanks to the source brightness and the use of confocal geometry, reaches the diffraction limit ($\lambda/2$) [19]. When combined with the latest technology and software developments of FTIR spectromicroscopy (notably 2D detectors), this technique gains a very large interest from bio-medicine investigators [17]. Synchrotron infrared microscopy has been successfully used in cell biology for the study of apoptotic and necrotic cells [20]. The study of the human cell responses to chemicals using FTIR spectromicroscopy has been performed [21]. This technique has also already been successfully used to assess the cells survival to chemotherapy [22].

In the present paper, we have combined confocal fluorescence and synchrotron infrared microcopies, on one hand, to localise the presence of HA inside the cells at various incubation periods and, on the other hand, to detect the associated biochemical modifications inside the cells following the addition of HA and the PDT at each incubation period. We have combined the results from the two techniques in order to better understand the PDT mechanism.

MATERIALS AND METHODS

Chemicals products

HA (Interchim, France) was dissolved in 100% DMSO at a concentration of 10^{-3} M and was stored in the dark at 4°C. All chemicals and media were purchased from Gibco-Invitrogen,

(Cergy Pontoise Cedex France).

Cell culture

HeLa cells were routinely cultured as monolayer and were grown in complete medium (Dulbecco's modified Eagle medium (DMEM) containing L-glutamine (862 mg/l), sodium pyruvate (110 mg/l) and glucose (4500 mg/l), supplemented with 10% fetal calf serum, penicillin (50 g/ml) and streptomycin (50 g/ml)) (CM). Cells were maintained at 37°C in a humidified atmosphere of 5% CO_2 and were fed every 3-4 days.

Photosensitizer localisation

Twenty four hours before incubation with HA, HeLa cells were seeded on 30 mm round coverglass in plastic Petri dishes (35 mm x 10 mm) at an optimal density of 10^5 cells/ml. HA was diluted appropriately in fresh culture medium to reach a final concentration in the cell culture of 2 µM. The final concentration of DMSO in the medium did not exceed 1% (in volume). HeLa cells were incubated with HA in the dark for the following time sequence: 0.5h, 1h, 2h, 3h, 5h, 24h at 37°C in a humidified atmosphere of 5% CO_2 in order to observe the HA intracellular uptake and distribution by confocal fluorescence microscopy.

Confocal fluorescence microscopy

After incubation, cells were washed twice with PBS and enclosed in a glass container in which medium was added to prevent cells from drying. The measurements were carried out on a laser scanning confocal microscope LSM 510 META (Carl Zeiss, Germany). For all measurements a C-Apochromat 40x/1.2 water immersion objective was used. As HA

exhibits a strong absorption band at 470 nm and an emission maximum around 620 nm (Fig.2), the subcellular distribution of HA was mapped by recording the fluorescence emission of HA longer than 505 nm, using a LP 505 long pass filter in response to an excitation wavelength of 488 nm provided by an Argon ion laser. The most representative 2D images for each incubation time are presented in Fig.3 without any data treatment. Each experiment was done in triplicate.

The 3D reconstruction of HA distribution in single cells after 2h of incubation was done using Edit 3D V3.0 (Y. Usson & F. Parazza) over 14 slices. Adaptive wavelength filtering and volume cropping were performed before interpolation.

Photodynamic effects

HeLa cells at the initial concentration of 10^5 cells/ml were cultured on low-e slides (MirrIR, Kevley Technologies) in the Petri dish. After overnight, the old medium was replaced by fresh medium with a final concentration at 2μM of HA. Cells were then incubated at 37°C in a humidified atmosphere of 5% CO_2. Following each period of incubation, the culture medium was removed. The cells were illuminated using a blue LED (460 nm) (LUXEON, USA), in the excitation maximum band of hypocrellin. Various doses of light have been used in this study, and it was found out, following MTT assays (data not shown) that the optimum dose was 10 $J.cm^{-2}$. After light illumination, cells were fixed with 4% formalin in PBS for 20 min at room temperature, and then rinsed for few seconds with distilled water. The fixed cells were dried and kept in a desiccator before being transported to the FTIR microscope beamline [23].

Infrared microspectroscopy

The experiments were performed at the infrared beamline, ID21, European Synchrotron Radiation Facility (Grenoble). The IR spectra were collected in reflection mode using an infrared microscope (Continu m-Thermo Electron Corporation) coupled to a FTIR spectrometer (Nicolet Nexus 870). The IR microscope is equipped with a motorized sample stage (precision 0.5 micron) and a liquid nitrogen cooled mercury cadmium telluride (MCT) detector- 50 microns size. All spectra were taken in reflection mode, and MirrIR low-e microscope slides were used as substrate. Each spectrum was acquired after 128 accumulations at 8 cm^{-1} spectral resolution. Data acquisition and processing were performed using Omnic software (Version 7.3, Thermo Electron Corporation). The average current in the storage ring was about 190 mA.

Each individual cell was selected visually and the IR spectra were taken at the nucleus location of the cell with an aperture of 6x6 μm^2. The reference spectrum was recorded with the same parameters and conditions, but outside the cells. Source stability was found exceptionally good all along the course of our experiments (RMS noise of 0.09 % between 2000 and 2200 cm^{-1}, for 128 scans at 8 cm^{-1} resolution, and for an aperture of 6x6 μm^2).

Data processing

Principal Component Analysis (PCA) was applied to infrared spectra for handling large data sets without preliminary assumption (also named unsupervised approach). PCA is a powerful chemometric method to reveal variances or combination of variables among

multivariate data. The computation of PCA is based on Non-linear Iterative Projections by Alternating Least-Squares (NIPALS) algorithm. In PCA, the raw data matrix X (n samples times m wavenumbers) is centered and split into a sum of matrix product TP^T and a residual matrix E.

$X = TP^T + E$ (1)

Where T is the score matrix and P^T the corresponding loading matrix transposed. The score vectors represent the footprints of the objects projected down onto the principal components and the loadings vectors can be viewed as the bridge between the variable space and principal component space. The characteristic absorption bands were revealed by studying the spectral patterns derived from the loadings plots.

The PCA classification was performed using the following: Since most of the spectra have marked baseline change over the entire frequency range, due to Mie scattering, it was necessary to get rid of this slow baseline change. We have first, smoothed the spectra using a Savitsky-Golay (SG) 3 points process, followed by first derivative and range normalisation (The Unscrambler, CAMO Process AS, Norway). The spectral domain has been reduced to 900-1800cm^{-1}. Then, a second data set was created by smoothing all the raw spectra with a SG 9 points, followed by second derivative and range normalisation. Typical raw, first derivative and second derivative spectra are displayed on Fig.4 . The PCA classification was validated only when both approaches have provided equivalent clustering.

Spectroscopic characterization of HA

The absorption spectrum of HA in DMSO solution was recorded using a UVIKON XL

absorption spectrometer (Serlabo, France). The fluorescence spectrum was recorded using a Jobin-Yvon Spectromax II (France). FTIR spectra of HA crystals were taken as described above.

RESULTS AND DISCUSSION

Photosensitizer localisation

The absorption and fluorescence emission spectra of HA in DMSO are displayed on Fig.2. The absorption maximum is observed at 470 nm. Accordingly, this absorption wavelength was selected for the induction of the photodynamic effect.

HeLa cells were incubated in an HA solution of 2 μM, as a function of time. The corresponding confocal fluorescence images are displayed on Fig. 5. All experiments were performed in the dark in order to avoid any photodynamic effect. Whatever incubation time, it appears quite clearly that HA distribution is restricted inside the cytoplasm and the perinuclear clustering. The fluorescence signal increases in intensity with longer incubation time up to 5 hours. After 5 hours of incubation, HA localises mainly in the perinuclear region, in agreement with previous studies [10, 11, 24]. A 3D image of the HA localisation of HA in HeLa cells is displayed on Fig.5 (g). After 24 hours of incubation, the fluorescence intensity inside cells decreases, probably due to an efflux of HA or a very high aggregation level of the drug leading to its fluorescence quenching [25].

The fluorescence microscopic study of HA has revealed that this drug does not penetrate inside the cell nucleus. It appears therefore, that a combined study with infrared microscopy, targeting more particularly the nucleus of HA cells, is necessary to provide a

deeper understanding of the interaction mechanisms.

Photodynamic effects

In order to study the biochemical changes occurring during the photodynamic effects, synchrotron based infrared microscopy has revealed to be a unique tool for the analysis of the nucleus of the treated cells.

To validate this technical approach, we have carried out two experiments. In the first study, we have recorded spectra of the same cell but at various aperture size centered on the center of the cell (Fig. 6). It becomes evident that the amide I band exhibits an upward frequency shift when the aperture used for recording the infrared spectrum increases over a value of 6x6 mm^2. This is, roughly, the average size of the HeLa cell nucleus. This behavior can be interpreted as a higher contrast provided by recording spectra in sub-regions of the cell containing mainly the nucleus, especially thanks to the confocal geometry allowed by the use of the synchrotron source. At larger aperture, an averaging of the infrared signal modifies the band position of the amide I. In the second experiment, we have recorded 100 spectra of individual HeLa cells for each case studied, namely control cells, incubated in 10 M HA solution, and subsequently illuminated with the light dose of 10 $J.cm^{-2}$ at 460 nm wavelength (data not shown). For each cell, two spectra were recorded, one in the cytoplasm, and one in the nucleus, using a 6x6 m^2 aperture (Fig.7). PCA of all the recorded spectra clearly shows a marked difference between spectra recorded inside the nucleus and those collected inside the cytoplasm (Fig.8). Analysis of PC1 loadings show that

different protein secondary structures are revealed between the nucleus and cytoplasm (Fig.9), with a more pronounced β–type secondary structure inside the nucleus.

It is worth remembering that a secondary structure change inside the nucleus has been suggested to correlated with the cell apoptosis as well as the cell death [21, 22].

In the FTIR-microspectroscopy investigation of the PDT-treated cells, the vibrational features associated by the presence of HA inside the cells were not observed, due the very weak concentration of HA, well below the detection limit in infrared spectroscopy.

Control cells and cells incubated in HA during three different times (30 minutes, 6 hours and 24 hours) have been first studied, in targeting specifically the nucleus of the cells, using an aperture of 6x6 μm^2.

We have carried out a PCA on control cells, as well as HA treated cells at various incubation times, none of them has been illuminated after incubation. The score plot of the two main principal components is displayed on Fig.10. No marked differences are seen in this score plot, meaning that no clear biochemical changes are noticed. PCA can, however, revealed subtle differences among those cells by plotting the higher order principal component, as shown on Fig.11. Along the PC3 axis, some of the treated cells are grouped on positive values of PC3. Note that most of the control cells lie in the negative value along the PC3 axis. The loadings plot (Fig.12) indicates that tiny changes in the secondary structure of the proteins are the main variables of the different groupings along the PC3 axis. The slight change in the secondary structure of some of the HA treated cells (beta sheets –related feature at 1630 cm^{-1}) may be explained by the change of the membrane protein structure upon penetration of HA inside the cells ; the high affinity of peryloquinone for membrane proteins has been only demonstrated in vitro with Glutathione S transferase [26].

The exposure of the HA-treated cells with light clearly shows the effect of the illumination on the cells. After incubation in HA, at various times, followed by exposure to a 10 $J.cm^{-2}$, the effect of illumination is clearly observed in the score plot displayed on Fig.13. Most of the cells, after 6h HA incubation time, followed by exposure to a 460 nm wavelength excitation, have a score clearly separated from the non-illuminated cells. On the Fig.13, scores are lying in the negative values of PC1. Indeed, we observed that several cells have not been affected by the light illumination. This may be understood as a non-homogeneous illumination or number of cell population.

The loading plot of PC1 is reported on Fig.14, between 1380 and 1800 cm^{-1}. These bands originate from the vibrations of the amide groups (CO-NH) of proteins. The peak of amide I at 1650 cm^{-1} is assigned to the α-helix structure of proteins while the peak of amide I at 1630 cm^{-1} to the β-sheet structure of proteins. Holman et al. [27] reported that the shift of amide I peaks to the lower energy showed the hallmark characteristics of cell death. The shifts found in our studies can be interpreted as originating from conformational differences in proteins in the HA-treated and PDT-treated cancer and control cells. The overall secondary structure of protein backbone changes are probably caused by the photodynamic effect of HA.

The effect of the light exposure can be, then, understood as, primarily, a marked change of the secondary structure of the proteins, which exhibits a pronounced linewidth change of the Amide I massif. The linewidth increases towards the low frequency region, and is interpreted as a higher contribution of beta-sheet secondary structure inside the cell nucleus, after illumination.

The representative spectra of control cells and 6h PDT treated cells are represented on Figure 15. It could be explained that DNA in treated cells can be packed tightly since DNA condensation, which is an important characteristic of apoptosis induced by PDT, has been observed under transmission electron microscope [4]. Moreover, the biochemical studied on the effect of PDT has described that PDT can induce apoptosis [28, 29]. However, it has been mentioned that the IR absorption of DNA depends on the activities of cells such as cell division, metabolic activities and chromatin condensation [15, 30]. The lower IR intensity of DNA may decrease due to a higher optical density [15].

FTIR microspectroscopy shows indirectly the effects of the drug at different incubation times but does not give clues concerning its localisation while, at the same time fluorescence microscopy allows to directly localise the drug. Both techniques are necessary to obtain a complete view of the pharmacokinetic of a drug at a cellular level.

The results from this study show the capability of FTIR microspectroscopy to study the effects of PDT on HeLa cells, showing indirect effects of the drug at individual cell level. Complementarily, fluorescence microscopy shows the intracellular distribution of HA in the cells. The combination of fluorescence microscopy with FTIR microspectroscopy at the cellular level enhances our understanding of the cancer cells response to treatments. Most photosensitizers are fluorescent molecules. While fluorescence microscopy is a powerful tool to investigate their distribution and pharmacokinetic mechanism at the subcellular level, the interactions and activity level are more accessed using a vibrational technique.

ACKNOWLEDGEMENTS

Royal Thai government scholarship from the ministry of science and technology, Thailand is gratefully acknowledged by Sirinart Chio-Srichan. We warmly thank Dr. Jean-Claude Drapier and his colleagues from the Institut de Chimie des Substances Naturelles, France for making the cell culture laboratory available to us. We also would like to thank Dr. Jean Susini and Dr. Marine Cotte, from ID21 beamline (European Synchrotron radiation Facility) for their assistance during the synchrotron infrared microscopy measurements. Dr. Josep Sulé-Suso and Dr. Ganesh D. Sockalingum are deeply acknowledged for their advices and fruitful discussions.

REFERENCES

[1] M.R. Hamblin and T. Hasan, Photodynamic therapy: a new antimicrobial approach to infectious disease?, Photochem. Photobiol. Sci. 3 (2004) 436-450.

[2] R.D. Almeida, B.J. Manadas, A.P. Carvalho and C.B. Duarte, Intracellular signalling mechanisms in photodynamic therapy, Biochim. Biophys. Acta 1704 (2004) 59-86.

[3] H.Y. Lee, Z.X. Zhou, S. Chen, M.-H. Zhang and T. Shen, New long-wavelength ethanolamino-substituted hypocrellin: photodynamic activity and toxicity to MGC803 cancer cell, Dyes and Pigments 68 (2006) 1-10.

[4] J. Zhang, E.H. Cao, J.F. Li, T.C. Zhang and W.J. Ma, Photodynamic effects of hypocrellin A on three human malignant cell lines by inducing apoptosis cell death, Photochem. Photobiol. 43 (1998) 106-111.

[5] J.B. Hudson, J. Whou, J. Chen, L. Harris, L. Yip and G.H.N. Towers, Hypocrellin, from

Hypocrella bambuase, is phototoxic to human immunodeficiency virus, Photochem. Photobiol. 60 (1994) 253-255.

[6] Z. Diwu, Novel therapeutic and diagnostic applications of hypocrellins and hypericins, Photochem. Photobiol. 61 (1995) 529-539.

[7] J. Hirayama, K. Ikebunchi, H. Abe, K. Kwon, Y. Ohnishi, M. Horiuchi, M. Shinagawa, K. Ikuta, N. Kamo and S. Sekiguchi, Photoinactivation of virus infectivity by Hypocrellin A, Photochem. Photobiol. 66 (1997) 697-700.

[8] Z. Diwu and J.W. Lown, Hypocrellins and their use in photosensitization, Photochem. Photobiol. 52 (1990) 609-616.

[9] Y.Y. He, J.Y. An and L.J. Jiang, pH effect on the spectroscopic behaviour and photogeneration of semiquinone anion radical of hypocrellin B, Dyes Pigments 41 (1998) 41-79.

[10] G.G. Miller, K. Brown, R.B. Moore, Z.J. Diwu, J. Liu, L. Huang, J.W. Lown, D.A. Begg, V. Chlumecky, J. Tulip and M.S. McPhee, Uptake kinetics and intracellular localisation of Hypocrellin photosensitizers for photodynamic therapy: a confocal microscopy study, Photochem. Photobiol. 61 (1995) 632-638.

[11] S.M. Ali and M. Olivo, Efficacy of hypocrellin pharmacokinetics in phototherapy, Int. J. Oncol. 21 (2002) 1229-1237.

[12] M. Jackson and H.H. Mantsch., Biomedical Infrared Spectroscopy, in (Wiley-Liss, ed.) Infrared Spectroscopy of Biomolecules, New York 1996, pp. 311.

[13] M. Jackson, J.R. Mansfield, R.L. Dolenko, R.L. Somorjai, H.H. Mantsch and P.H. Watson, Classification of breast tumors by grade and steroid receptor status using

pattern recognition analysis of infrared spectra Cancer Detect. Prev. 23 (1999) 245.

[14] H.H. Mantsch, L.P. Choo-Smith and R.A. Shaw, Vibrational spectroscopy and medicine: An alliance in the making, Vibrational Spectroscopy 30 (2002) 31-41.

[15] M. Diem, S. Boydston-White and L. Chiriboga, Infrared spectroscopy of cells and tissues: shining light onto an unsettled subject, Appl. Spectrosc. 53 (1999) 148A-168A.

[16] M. Jackson, J.R. Mansfield, R.L. Dolenko, R.L. Somorjai, H.H. Mantsch and P.H. Watson, Classification of breast tumors by grade and steroid receptor status using pattern recognition analysis of infrared spectra, Cancer Detect Prev. 23 (1999) 245.

[17] P. Dumas, G.D. Sockalingum and J. Sulé-Suso, Adding synchrotron radiation to infrared microspectroscopy: what's new in biomedical applications?, Trends in Biotechnology 25 (2006) 40-44.

[18] L.M. Miller and P. Dumas, Chemical imaging of biological tissue with synchrotron infrared light, Biochim. Biophys. Acta 1758 (2006) 846-857.

[19] G.L. Carr, Resolution limits for infrared microspectroscopy explored with synchrotron radiation, Review of Scientific Instruments 72 (2001) 1613-1619.

[20] N. Jamin, L.M. Miller, J. Montcuit, W.H. Fridman, P. Dumas and J.L. Teillaud, Chemical heterogeneity in cell death: combined synchrotron infrared and fluorescence microscopy studies of apoptotic and necrotic cells, Biopolymers (Biospectroscopy) 72 (2003) 366-373.

[21] H.N. Holman, R. Goth-Goldstein, M.C. Martin and W.R. McKinney, , Low-dose responses to 2,3,7,8-tetrachlorodibenzo-ρ-dioxin in single living human cells measured by synchrotron infrared spectromicroscopy, Environ. Sci. Technol. 34 (2000) 2513-2517.

[22] J. Sulé-Suso, D. Skingsley, G.D. Sockalinghum, A. Kohler, G. Kegelaer, M. Manfait and

A. El Haj, FTIR microspectroscopy as a tool to access lung cancer cells response to chemotherapy, Vibrational Spectrosocopy 38 (2005) 179-184.

[23] E. Gazi, J. Dwyer, N.P. Lockyer, J. Miyan, P. Gardner, C. Hart, M. Brown and N.W. Clarke, Fixation protocols for subcellular imaging by synchrotron-based fourier transform infrared microspectroscopy, Biopolymer 77 (2005) 18-30.

[24] W. Chin, W. Lau, C. Cheng and M. Olivo, Evaluation of hypocrellin B in a human bladder tumor model in experimental photodynamic therapy: biodistribution, light dose and drug-light interval effects, Int. J. Oncol. 25 (2004) 623-629.

[25] S. Kascakova, M. Réfrégiers, D. Jancura, F. Sureau, J.-C. Maurizot and P. Miskovsky, Fluorescence spectroscopic study of hypericin-photosensitized oxidation of low-density lipoproteins, Photochem. Photobiol. 81 (2005) 1395-1403.

[26] M. Halder, P.K. Chowdhury, R. Das, P. Mukherjee, W.M. Atkins, J.W. Petrich, Interaction of glutathione S-transferase with hypericin : A photophysical study, J. Phys. Chem. B 109 (2005) 19484-19489.

[27] H.N. Holman, M.C. Martin, E.A. Blakely, K. Bjornstad and W.R. McKinney, , IR spectroscopic characteristics of cell cycle and cell death probed by synchrotron-based FTIR microspectroscopy, Biopolym. Biospectrosc. 57 (2000) 329-335.

[28] H. Yang, T. Wu, M. Zhang and Z. Zhang, A novel photosensitizer, 2-butylamino-2-demethoxy-hypocrellin B (2-BA-2-DMHB)-its photodynamic effects on HeLa cells: efficacy and apoptosis, Biochim. Biophys. Acta 1540 (2001) 22-31.

[29] S. Xu, S. Chen, M. Zhang, T. Shen, Y. Whao, Z. Liu and Y. Wu, Butylamino-demethoxy-hypocrellins and photodynamic therapy decreases human cancer in vitro and in vivo, Biochim. Biophys. Acta 1537 (2001) 222-232.

[30] S. Boydston-White, T. Chernenko, A. Regina, M. Miljković, C. Matthäus and M. Diem, Microscopy of single proliferating HeLa cells, Vibr. Spectrosc. 38 (2005) 169-177.

LEGENDS :

Fig. 1: Chemical formula of Hypocrellin A.

Fig.2 : Absorption and Emission spectra of Hypocrellin A.

Fig. 3: Confocal fluorescence images of HeLa cells recorded after increasing incubation time in a solution of 2 M of HA (a) 30 minutes; (b) 1 hour ; (c) 2 hours ; (d): 3 hours ; (e) : 5 hours ; (f): 24 hours. 3D reconstruction of the intracellular localisation of HA after 2 hours incubation, color coded for z.

Fig. 4: (A) Raw spectrum ; (B) First derivative spectrum following a Savisky-Golay , 3 points smoothing, and (C) Second derivative spectrum following a Savisky-Golay , 9 points smoothing. First and second derivative spectra have been used for PCA classification.

Fig.5 : Infrared spectra recorded on the same cell, at different size of the projected aperture centered on the single cell. A marked change in the amide I band shape is evident for aperture below 6x6 μm^2. This corresponds to the average size of the nucleus. This shows that the use of confocal geometry, combined with the high brightness of the synchrotron source, has revealed a specific secondary structure of the proteins inside the cell nucleus.

Fig.6 : Probing area inside HeLa cells using synchrotron infrared microscopy. The dimension of the projected aperture onto the samples set to 6x6 μm^2 (represented as a dashed

square), allows probing either the nucleus or the cytoplasm of each cell.

Fig.7: PCA analysis of the whole set of spectra taken inside the nucleus and the cytoplasm of about 100 cells. There is a clear separation of spectra into two clusters, as shown in the figure, the discrimination is 92% accounted along the PC1 axis.

Fig.8: Loadings plot of PC1 and PC2 , showing that for spectra lying along the negative values of PC1 axis,beta-sheets vibrational bands are responsible for the marked loading difference, as manifested by the peaks at 1630 and 1520 cm^{-1}, and are predominantly located inside the nucleus. PC2 loadings (7% variance) is also shown to strengthen our results.

Fig.9: PCA analysis of the whole set of spectra taken inside the nucleus: score plot of PC2 versus PC1 for controlled cells (dark circle), incubated in HA during 30 minutes (dark square), 6 hours (open square) and 24 hours (open circle).

Fig.10: Score plot of PC3 versus PC1 of the same spectra set as for Fig.7. While all of the spectra recorded in controlled cells (dark circle) lies in the negative values of PC3, several spectra recorded on HA incubated cells during 30 minutes (dark square), 6 hours (open square) and 24 hours (open circle), are markedly clustered for positive values of PC3.

Fig.11: Loading plot of PC3 showing the main features which contribute mainly to the

variability.

Fig.12 Score plot PC2 versus PC1 for control cells (dark circle), HA incubated in dark during 30 minutes (dark square), 6 hours (open squares), 24 hours (open circle) and cells incubated in HA during 6 hours , followed by illumination with a dose of 10 $J.cm^{-2}$ (open triangle).

Fig.13 Loading plot of PC1, corresponding to the score plot of Fig.10.

Fig.14 Average spectra over the frequency region 900-1800 cm^{-1}, of cells incubated in HA during 6 hours, in the dark, and after being irradiated with 10 J. cm^{-2} at 460 nm wavelength.

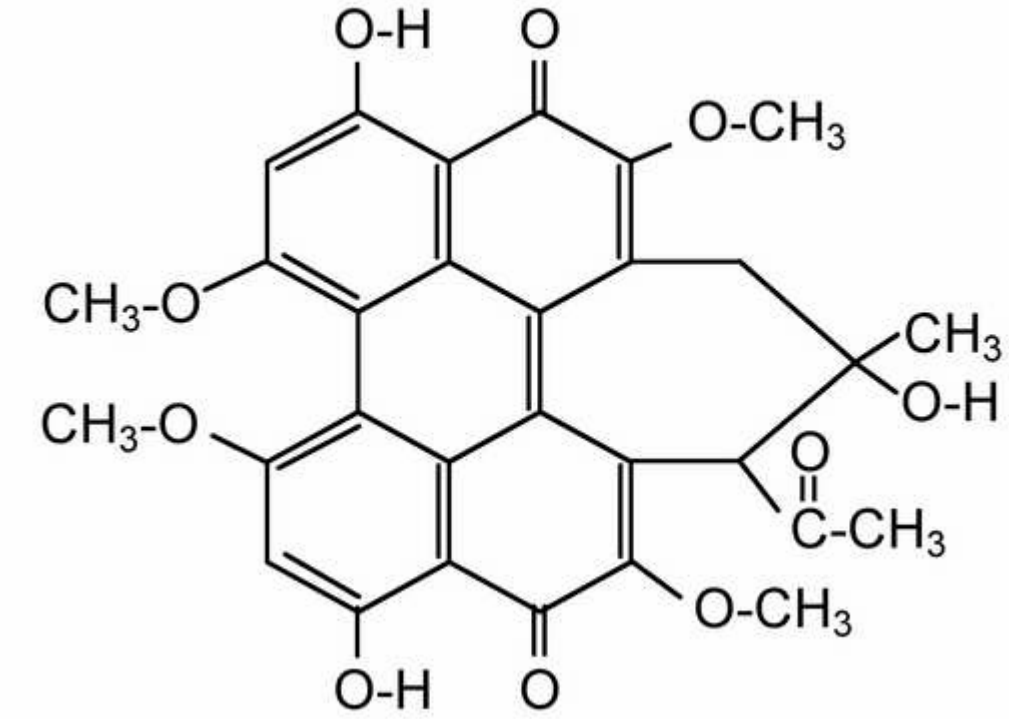

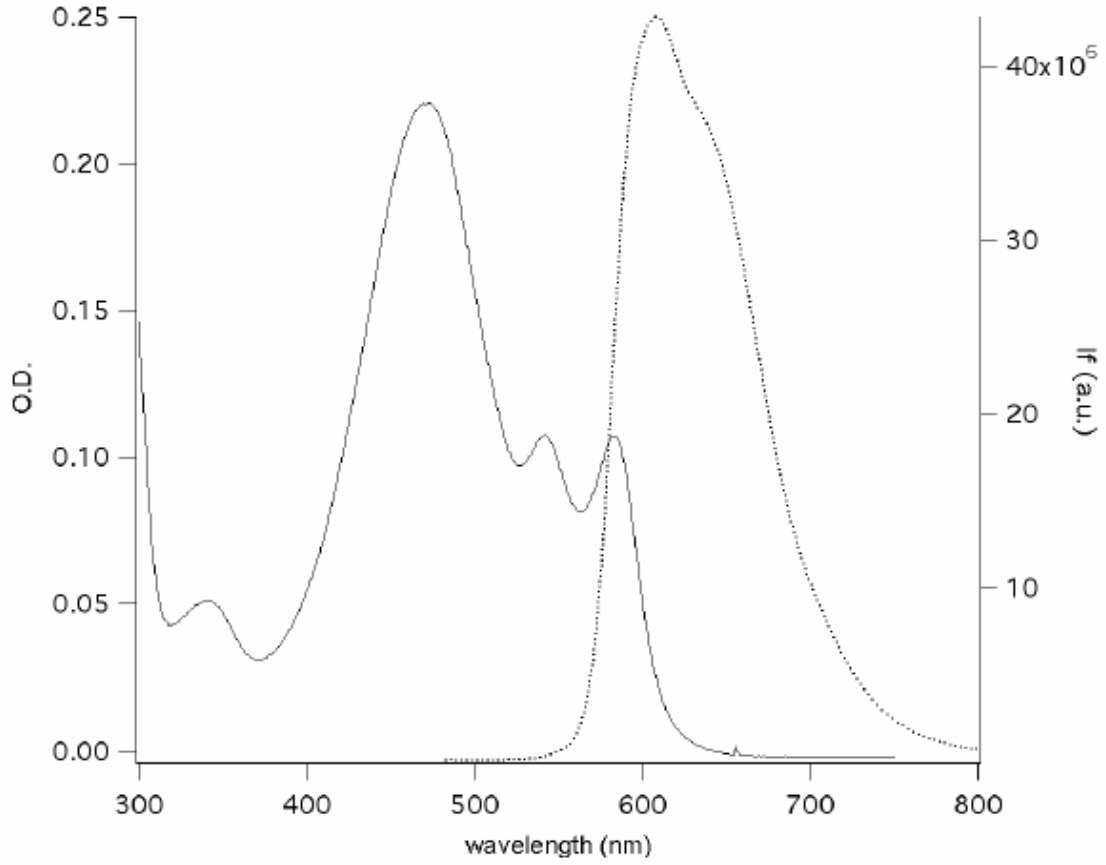

Fig.2